

Exploring Quantum Physics at the ILC

A. FREITAS^{1*}, K. HAGIWARA^{2†}, S. HEINEMEYER^{3‡}, P. LANGACKER^{4,5§},
K. MOENIG^{6¶}, M. TANABASHI^{7,8||} AND G.W. WILSON^{9**}

¹*Pittsburgh Particle physics, Astrophysics, and Cosmology Center, Department of Physics
& Astronomy, University of Pittsburgh, Pittsburgh, PA 15260, USA*

²*KEK Theory Center and Sokendai, Tsukuba 305-0801, Japan*

³*Instituto de Física de Cantabria (CSIC-UC), Santander, Spain*

⁴*Institute for Advanced Study, Princeton, NJ 08540, USA*

⁵*Department of Physics, Princeton University, Princeton, NJ 08544, USA*

⁶*DESY Zeuthen, Germany*

⁷*Kobayashi-Maskawa Institute for the Origin of Particles and the Universe, Nagoya
University, Nagoya 464-8602, Japan*

⁸*Department of Physics, Nagoya University, Nagoya 464-8602, Japan*

⁹*Department of Physics and Astronomy, University of Kansas, Lawrence, KS 66045, USA*

Abstract

We review the ILC capabilities to explore the electroweak (EW) sector of the SM at high precision and the prospects of unveiling signals of BSM physics, either through the presence of new particles in higher-order corrections or via direct production of extra EW gauge bosons. This includes electroweak precision observables, global fits to the SM Higgs boson mass as well as triple and quartic gauge boson couplings.

*email: afreitas@pitt.edu

†email: kaoru.hagiwara@kek.jp

‡email: Sven.Heinemeyer@cern.ch

§email: pgl@ias.edu

¶email: klaus.moenig@desy.de

||email: tanabash@eken.phys.nagoya-u.ac.jp

**email: gwwilson@ku.edu

1 Introduction

The Standard Model (SM) cannot be the ultimate fundamental theory of particle physics. So far, it succeeded in describing direct experimental data at collider experiments exceptionally well with only a few notable exceptions, e.g., the left-right ($A_{\text{LR}}^e(\text{SLD})$) and forward-backward ($A_{\text{FB}}^b(\text{LEP})$) asymmetry, and the muon magnetic moment $(g-2)_\mu$. However, the SM fails to include gravity, it does not provide cold dark matter, and it has no solution to the hierarchy problem, i.e. it does not have an explanation for a Higgs-boson mass at the electroweak scale. On wider grounds, the SM does not have an explanation for the three generations of fermions or their huge mass hierarchies. In order to overcome (at least some of) the above problems, many new physics models (NPM) have been proposed and studied, such as supersymmetric theories, in particular the Minimal Supersymmetric Standard Model (MSSM), Two Higgs Doublet Models (THDM), Technicolor, little Higgs models, or models with (large, warped, or universal) extra spatial dimensions.

If a direct discovery of new BSM particles is out of reach at the LHC and/or the ILC, precision measurements of SM observables have proven to be a powerful probe of NPM via virtual effects of the additional NPM particles. In general, precision observables (such as particle masses, mixing angles, asymmetries etc.) that can be predicted within a certain model, including higher order corrections in perturbation theory, and thus depending sensitively on the other model parameters, and that can be measured with equally high precision, constitute a test of the model at the quantum-loop level. Various models predict different values of the same observable due to their different particle content and interactions. This permits to distinguish between, e. g., the SM and a NPM, via precision observables. Naturally, this requires a very high precision of both the experimental results and the theoretical predictions.

We review the ILC capabilities to explore the electroweak (EW) sector of the SM at high precision and the prospects of unveiling signals of BSM physics, either through the presence of new particles in higher-order corrections or via direct production of extra EW gauge bosons. We discuss the experimental and theory uncertainties in the measurement and calculation of electroweak precision observables (EWPO), such as the W boson mass and Z pole observables, in particular the effective weak mixing angle, $\sin^2 \theta_{\text{eff}}^\ell$. As an example for BSM physics the MSSM is a prominent showcase and will be used here for illustration.

The recent discovery of a Higgs-like particle at the LHC has a profound impact on EW precision tests of the SM. We review the results of a global EW fit including ILC precision and discuss also the relevance of a precise top quark mass determination.

We review the anticipated accuracies for precision measurements of triple and quartic EW gauge boson couplings. These observables are of special interest at the ILC, since they have the potential of accessing energy scales far beyond the direct kinematical reach of the LHC or the ILC. Finally, we discuss the ILC reach for a discovery of extra EW gauge bosons, Z' and W' .

2 The ILC Project Overview

Following an intense and successful R&D phase, the ILC has now achieved a state of maturity and readiness, culminating recently with the publication of the Technical Design Report [1]. Several important physics goals at the TeV energy scale have motivated this effort. These include precision measurements of the properties of the recently discovered Higgs-like boson, including its couplings to fermions and bosons, improving knowledge of the top quark to a high level of precision, and the search for signals of new physics through the electroweak production of new particles and indirectly through precision measurements of W , Z , and two-fermion processes. The ILC experiments will be sensitive to new phenomena, such as supersymmetric partners of known particles, new heavy gauge bosons, extra spatial dimensions, and particles connected with strongly-coupled theories of electroweak symmetry breaking [2]. In all of these, the ILC will yield substantial improvements over LHC measurements and will have a qualitative advantage on signatures that have high backgrounds at LHC or are difficult to trigger on. Detailed simulations with realistic detector designs show that the ILC can reach the precision goals needed [3]. Just as the LHC experiments are now making more precise measurements than were originally predicted (as was also the case with the Tevatron, LEP and SLC experiments), the ILC experiments will bring qualitatively new capabilities and should similarly exceed the performance levels based on current simulations when data are in hand.

The requirements of the ILC [4] include tunability between center-of-mass energies of 200 and 500 GeV, with rapid changes in energy over a limited range for threshold scans. The luminosity, which must exceed $10^{34} \text{ cm}^{-2}\text{s}^{-1}$ at 500 GeV, roughly scales proportionally with center-of-mass collision energy. Highly polarized electrons ($> 80\%$) are specified, with polarized positrons desirable. The TDR design [1] has met these specifications. R&D has achieved the accelerating gradient goal of 35 MV/m in test stands and 31.5 MV/m in installed cryomodules with beam loading. Cavity fabrication to these specifications has been industrialized. The effects of the electron cloud in the positron damping ring have been studied experimentally, leading to proven techniques for its mitigation. Fast kickers needed for damping ring beam injection and ejection have been developed. The required small final focus spot size is being demonstrated in a test facility. The final focus and interaction region, including the detector push-pull system, has been designed. Two detailed detector designs have been developed [2], with R&D supporting these designs. Beam tests with highly granular calorimeters have demonstrated the calorimetry performance needed by using the particle flow technique. Similarly, tracking R&D has advanced for vertex detection based on thin CMOS monolithic pixel sensors, outer tracking with low-mass supported silicon microstrips, and advanced TPC technologies employing micropattern gas detectors or silicon sensors for readout.

Recently, the Japanese government has expressed a desire to host the ILC, and international negotiations are underway. In a staged approach, beginning at a center-of-mass energy of 250 GeV, a physics program would start with precision measurements of the Higgs branching ratios and properties. Raising the energy to 500 GeV would move to precision measurements of top quark properties well beyond those possible at the LHC. Measurements of the top coupling to the Higgs and the Higgs self coupling would begin at 500 GeV. Should there be accessible new particles such as supersymmetric partners of gauge bosons and lep-

tons, the ILC is the only place where they can be studied in full detail. If there are multiple Higgs bosons, the ILC would be needed to measure their branching fractions and the mixing angle $\tan \beta$. Extension of the ILC to 1 TeV is straightforward, with lengthened linac tunnels and additional cryomodules, building on the original ILC sources, damping rings, final focus and interaction regions, and beam dumps.

3 Experimental considerations

Experiments at e^+e^- colliders play leading roles in our current understanding of nature. The experimental techniques, conditions and detectors allow the experimenter to investigate the science in a direct, largely model-independent and above all simple manner.

The ILC detectors and the ILC facility offers the potential to advance particle physics with an unparalleled science opportunity. The ILC *linear* collider is capable of operating over an extensive range of center-of-mass energies colliding point-like particles at $\sqrt{s} = 91 - 1000$ GeV with high luminosity. The beam energies are easily tuned to allow threshold scans for precision mass measurements. The electron beam can be polarized to 80-90% and the positron beam can also be polarized to 30-60%. Longitudinal polarization is very important [5]. Since in the Standard Model the left- and the right-handed electron belong to different multiplets this gives access to completely different couplings. It also serves as a method to enhance/decrease particular processes. An often occurring example is the utility of either enhancing or decreasing the contribution of WW -fusion and WW production diagrams. In these respects, polarization is essentially a significant increase (up to a factor of 3) in the effective luminosity of the collider. Physics at an e^+e^- collider enjoys the luxury of “democratic” production of signal and background leading to very favorable signal to background ratios even for processes such as those with hadronic final states which can be buried under many orders of magnitude of QCD background at the LHC.

The ILC experimental outlook is one of a scientific facility which will significantly exceed the capabilities of the previous generation of experiments such as LEP and SLC. It is in many respects targeting much higher performance than is achievable in a hadron collider environment. A distinct advantage of the ILC linac technology is the time structure of the colliding bunches. The time between bunches (366 ns), the 199 ms quiet time between bunch trains and current technologies lead to a data acquisition approach which will greatly benefit the physics. There is no need for a hardware-based fast trigger nor concerns on overall data volume. Furthermore the pulse structure with the possibility of power-pulsing and the lack of significant radiation hardness constraints, means that for many subdetector designs the material thicknesses can be minimized or the technology with the best performance chosen, leading to better performance and a more hermetic detector. Detector backgrounds are well understood and not a serious impediment to experimentation.

These conditions allow the deployment of state-of-the-art pixellated vertex detectors, large volume thin Silicon tracking, a new generation Time Projection Chamber (TPC), ultra-high granularity calorimetry designed from the outset for particle-flow based jet reconstruction, and allows hermetic coverage to forward angles (around 10 mrad). This results in superb vertex-tagging of b -quarks, c -quarks and τ leptons, exquisite momentum resolution, jet energy resolution allowing the separation of hadronically-decaying W and Z bosons, and

detection of significant missing energy in low visible energy final states. The vision is to have bubble-chamber like event reconstruction with high multiplicity final states and essentially no significant background from multiple interactions. The detectors promise outstanding performance which should be capitalized on by ensuring that experimental issues like detector stability, alignment, calibration, magnetic field mapping, jet energy scale, momentum scale will be under correspondingly good control.

An extremely important aspect of an e^+e^- collider is the knowledge, precise measurement and monitoring of the initial-state beam parameters. Essential quantities to control as well as possible are: the beam energy, the center-of-mass energy, beam polarizations, luminosity, integrated luminosity, the luminosity spectrum, the beam energy spread and the beam-spot. When these are well controlled the physics benefits are significant. Firstly, a well understood integrated luminosity improved to that what was achieved at LEP (0.034% experimental error) allows precision tests of all absolute cross-section measurements with corresponding theoretical calculations. This aspect of outstanding absolute normalization of experimental measurements and the of the dominantly electroweak based theory calculations, means that even very small deviations can be detected. It also has great benefits in the direct search for new physics. Secondly, when the distributions of the initial state four-momenta are well measured, one can in many circumstances take advantage of the kinematic constraints of energy and momentum conservation. Both of these major advantages are foreseen for the ILC, and significant preparatory work has already established the feasibility of quality knowledge of the beam parameters. See for example [6] for related work on applying kinematic constraints.

One of the new features of ILC compared to LEP and SLC is that the highly focused beams (several nm vertical beam size) lose on average a few per-cent of their energy through the emission of beamstrahlung photons as a result of the beam-beam interaction. The overall effect for ILC is small on the scale of initial state radiation but must be measured directly from collision events such as Bhabha scattering events [7].

When electron and positron polarization is available the beam polarization can be measured from data in a model independent way and polarimeters are needed only for small corrections. Also the beam energy can be calibrated relative to the Z-boson mass which is known from LEP with a precision of 2.1 MeV. To go beyond this precision an absolute beam energy measurement on the 10^{-5} level is needed which seems difficult.

The ILC will run in several distinct phases. Initially the ILC will run at a center of mass energy around 250 GeV for a precise measurement of the Higgs couplings and then gradually increase its energy via the top-pair threshold at 350 GeV to its maximum value. From the beginning runs at the top of the Z-resonance will be needed to calibrate the energy scale of the detector. At a later stage a long run at the Z pole is foreseen to collect about 10^9 Z decays for a measurement of the effective weak mixing angle with ultimate precision. This run also requires a scan of the resonance which might also be used to improve the knowledge of the Z width. If it turns out to be interesting the W-mass measurement can be improved with a dedicated scan of the W-pair production threshold around 160 GeV.

Some of the relevant beam parameters are shown in Tab. 1 for the default TDR parameter sets used in the TDR full simulation studies. It should be noted that the momentum spread at 200 GeV is very similar to LEP2.

| \sqrt{s} | $\mathcal{L}[10^{34}]$ | dE [%] | (dp/p)(+) [%] | (dp/p)(-) [%] |
|------------|------------------------|--------|---------------|---------------|
| 200 | 0.56 | 0.65 | 0.190 | 0.206 |
| 250 | 0.75 | 0.97 | 0.152 | 0.190 |
| 350 | 1.0 | 1.9 | 0.100 | 0.158 |
| 500 | 1.8/3.6 | 4.5 | 0.070 | 0.124 |
| 1000 | 4.9 | 10.5 | 0.047 | 0.085 |

Table 1: Relevant beam parameters for the ILC as a function of \sqrt{s} . Given are the luminosity, the average energy loss from beamstrahlung, average center-of-mass energy spread from momentum spread.

4 Electroweak precision observables

4.1 The W boson mass

The mass of the W boson is a fundamental parameter of the electroweak theory and a crucial input to electroweak precision tests. The present world average for the W -boson mass [8],

$$M_W^{\text{exp}} = 80.385 \pm 0.015 \text{ GeV} , \quad (1)$$

is dominated by the results from the Tevatron, where the W boson mass has been measured in Drell–Yan-like single- W -boson production. At LEP2, the W -boson mass had been measured in W -pair production with an error of 33 MeV from direct reconstruction and ~ 200 MeV from the cross section at threshold [9].

The three most promising approaches to measuring the W mass at the ILC are:

- Polarized threshold scan of the W^+W^- cross-section as discussed in [10].
- Kinematically-constrained reconstruction of W^+W^- using constraints from four-momentum conservation and optionally mass-equality as was done at LEP2.
- Direct measurement of the hadronic mass. This can be applied particularly to single- W events decaying hadronically or to the hadronic system in semi-leptonic W^+W^- events.

Each method can plausibly measure M_W to an experimental precision in the 5 – 6 MeV range. The three methods are largely uncorrelated. If all three methods do live up to their promise, one can target an overall uncertainty on M_W in the range of 3 – 4 MeV.

The anticipated experimental accuracy has to be matched with a theoretical uncertainty at the same level of accuracy. This is particularly challenging for the WW threshold scan, where a full diagrammatic calculation of $e^+e^- \rightarrow 4f$ and leading two-loop corrections are required, see Refs. [11, 12] and references therein. All building blocks for a sufficiently precise prediction of the W -pair production cross section in the threshold region are available. They require the combination of the NLO calculation of the full four fermion cross section with the (parametrically) dominant NNLO corrections, which are calculated within the EFT. For the

precise determination of the cross section at energies above 500 GeV the leading two-loop (Sudakov) corrections should be included in addition to the full NLO corrections. Combining the theoretical uncertainties with the anticipated precision from a threshold scan (see the previous subsection) a total uncertainty of 6 MeV can be estimated (see also Ref. [13]). For the overall future experimental uncertainty we arrive at

$$\delta M_W^{\text{exp,ILC}} = 5 - 6 \text{ MeV} . \quad (2)$$

The currently most accurate theoretical prediction of M_W in the SM is based on a full two-loop calculation, supplemented with leading corrections at the three- and four-loop level, entering via the ρ -parameter, see Ref. [14] for a review (and references therein). The total intrinsic uncertainty from unknown higher-order corrections has been estimated to [15]

$$\delta M_W^{\text{SM,theo}} = 4 \text{ MeV} . \quad (3)$$

This error mainly stems from missing $\mathcal{O}(\alpha^2\alpha_s)$, $\mathcal{O}(N_f^3\alpha^3)$ and $\mathcal{O}(N_f^2\alpha^3)$ contributions, where N_f^n denotes diagrams with n closed fermion loops. These are expected to be calculable in the foreseeable future using numerical methods or asymptotic expansions, leading to a remaining intrinsic uncertainty of

$$\delta M_W^{\text{SM,theo,fut}} \approx 1 \text{ MeV} . \quad (4)$$

Within the MSSM, due to the additional missing higher-order corrections the current intrinsic theory uncertainty increases to [16]

$$\delta M_W^{\text{MSSM,theo}} = 5 - 10 \text{ MeV} , \quad (5)$$

depending on the masses of the SUSY particles. In the future this could be reduced to

$$\delta M_W^{\text{MSSM,theo,fut}} = 3 - 5 \text{ MeV} . \quad (6)$$

The main SM parametric uncertainties are introduced by m_t , $\Delta\alpha_{\text{had}}$ and M_Z . Using today's values $\delta m_t = 0.9 \text{ GeV}$, $\delta(\Delta\alpha_{\text{had}}) = 10^{-4}$ and $\delta M_Z = 2.1 \text{ MeV}$, yields

$$\delta M_W^{\text{para},m_t} = 5.5 \text{ MeV}, \quad \delta M_W^{\text{para},\Delta\alpha_{\text{had}}} = 2 \text{ MeV}, \quad \delta M_W^{\text{para},M_Z} = 2.6 \text{ MeV} , \quad (7)$$

dominating the intrinsic theory uncertainties. They are reduced, however, if one assumes the ILC accuracy for m_t as given by Eq. (31), and an improvement to $\delta(\Delta\alpha_{\text{had}}) = 5 \times 10^{-5}$ by future low energy e^+e^- measurements,

$$\Delta M_W^{\text{para,fut},m_t} = 1 \text{ MeV}, \quad \Delta M_W^{\text{para,fut},\Delta\alpha_{\text{had}}} = 1 \text{ MeV} , \quad (8)$$

where no improvement in the measurement of M_Z is current foreseeable. Thus $\Delta M_W^{\text{para},M_Z}$ could dominate the future theoretical uncertainties. However, they would still stay below the anticipated ILC experimental accuracy as given in Eq. (2).

An example that demonstrates the power of the ILC precision in M_W , taken together with the top quark mass (see Sect. 4.3), is shown in Fig. 1. The evaluation of M_W includes

the full one-loop result and all known higher order corrections of SM- and SUSY-type, for details see [16, 17] and references therein. In the left plot the green region indicated the MSSM M_W prediction (as obtained from a 15-dim. parameter scan [17]), assuming the light \mathcal{CP} -even Higgs h in the region 125.0 ± 2 GeV. The blue band indicates the overlap region of the SM and the MSSM with $M_H^{\text{SM}} = 125.0 \pm 2$ GeV. The right plot shows the M_W prediction assuming the heavy \mathcal{CP} -even Higgs H in the region 125.0 ± 2 GeV. The red band indicates the SM region with $M_H^{\text{SM}} = 125.0 \pm 2$ GeV. The gray ellipse indicates the current experimental uncertainty, see Eqs. (1), (30), whereas the red ellipse shows the anticipated future ILC/GigaZ precision, assuming an uncertainty of 7 MeV for M_W and 0.1 GeV for m_t . While at the current level of precision SUSY might be considered as slightly favored over the SM by the M_W - m_t measurement, no clear conclusion can be drawn. The small red ellipses, on the other hand, indicate the discrimination power of the future ILC/GigaZ measurements. With the improved precision a small part of the MSSM parameter space could be singled out. The comparison of the SM and MSSM predictions with the ILC/GigaZ precision could rule out either of models.

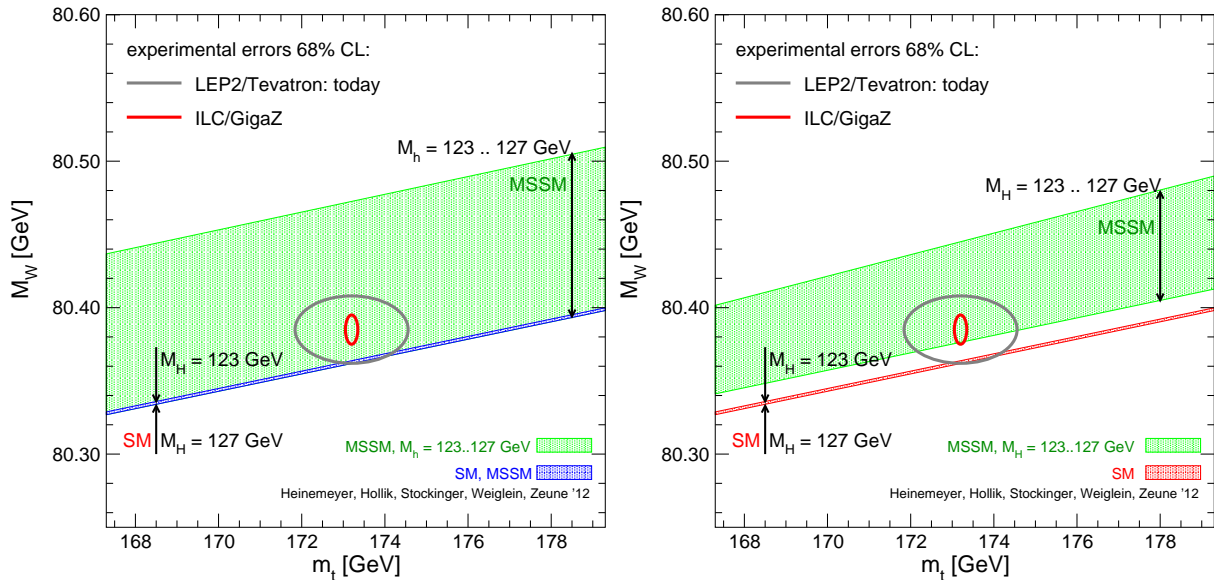


Figure 1: Prediction for M_W as a function of m_t . The left plot shows the M_W prediction assuming the light \mathcal{CP} -even Higgs h in the region 125.0 ± 2 GeV. The blue band indicates the overlap region of the SM and the MSSM with $M_H^{\text{SM}} = 125.0 \pm 2$ GeV. The right plot shows the M_W prediction assuming the heavy \mathcal{CP} -even Higgs H in the region 125.0 ± 2 GeV. The red band indicates the SM region with $M_H^{\text{SM}} = 125.0 \pm 2$ GeV. The gray ellipse indicates the current experimental uncertainty, whereas the red ellipse shows the anticipated future ILC/GigaZ precision.

4.2 The Z boson observables

Other important EWPOs are the various observables related to the Z boson, measured in four-fermion processes, $e^+e^- \rightarrow \gamma, Z \rightarrow f\bar{f}$, at the Z boson pole. Besides the improvements

in $\sin^2 \theta_{\text{eff}}^\ell$ (which will be discussed below in detail) and M_W , GigaZ has the potential to determine the total Z width within $\delta\Gamma_Z = \pm 1$ MeV; the ratio of hadronic to leptonic partial Z widths with a relative uncertainty of $\delta R_l/R_l = \pm 0.05\%$; the ratio of the $b\bar{b}$ to the hadronic partial widths with a precision of $\delta R_b = \pm 1.4 \times 10^{-4}$; and to improve the b quark asymmetry parameter A_b to a precision of $\pm 1 \times 10^{-3}$ [18, 19].

A special role is played by the effective weak leptonic mixing angle, $\sin^2 \theta_{\text{eff}}^\ell$, which can be determined via various measurements, in particular via the forward-backward (FB) asymmetry of b quarks, A_{FB}^b , and via the left-right (LR) asymmetry of electrons, A_{LR}^e . The current experimental uncertainty is given by [20]

$$\sin^2 \theta_{\text{eff}}^{\ell \text{ exp}} = 0.23153 \pm 0.00016 , \quad (9)$$

mainly driven by

$$A_{\text{FB}}^b(\text{LEP}) : \sin^2 \theta_{\text{eff}}^{\ell \text{ exp,LEP}} = 0.23221 \pm 0.00029 , \quad (10)$$

$$A_{\text{LR}}^e(\text{SLD}) : \sin^2 \theta_{\text{eff}}^{\ell \text{ exp,SLD}} = 0.23098 \pm 0.00026 . \quad (11)$$

At the ILC $\sin^2 \theta_{\text{eff}}^\ell$ can be measured running at the Z -mass (i.e. at GigaZ), using the left-right asymmetry [18]. With at least the electron beam polarised with a polarisation of \mathcal{P} , $\sin^2 \theta_{\text{eff}}^\ell$ can be obtained via

$$A_{\text{LR}}^e = \frac{1}{\mathcal{P}} \frac{\sigma_L - \sigma_R}{\sigma_L + \sigma_R} = \frac{2g_{V_e}g_{A_e}}{g_{V_e}^2 + g_{A_e}^2} \quad (12)$$

$$g_{V_e}/g_{A_e} = 1 - 4 \sin^2 \theta_{\text{eff}}^\ell \quad (13)$$

independent of the final state. g_{V_e} and g_{A_e} denote the vector and axial-vector couplings of the Z boson to electrons. With 10^9 Z bosons, an electron polarisation of 80% and no positron polarisation the statistical error is $\Delta A_{\text{LR}}^e = 4 \times 10^{-5}$. The error from the polarisation measurement is $\Delta A_{\text{LR}}^e/A_{\text{LR}}^e = \Delta\mathcal{P}/\mathcal{P}$. With electron polarisation only and $\Delta\mathcal{P}/\mathcal{P} = 0.5\%$ one has $\Delta A_{\text{LR}}^e = 8 \times 10^{-4}$, much larger than the statistical precision. If positron polarisation is also available \mathcal{P} in equation (12) has to be replaced by $\mathcal{P}_{\text{eff}} = \frac{\mathcal{P}_{e^+} + \mathcal{P}_{e^-}}{1 + \mathcal{P}_{e^+}\mathcal{P}_{e^-}}$. For $\mathcal{P}_{e^-}(\mathcal{P}_{e^+}) = 80\%(60\%)$ the error in \mathcal{P}_{eff} is a factor of three to four smaller than the error on \mathcal{P}_{e^+} , \mathcal{P}_{e^-} depending on the correlation between the two measurements. If one takes, however, data on all four polarisation combinations the left-right asymmetry can be extracted without absolute polarimetry [21] and basically without increasing the error if the positron polarisation is larger than 50%. Polarimetry, however, is still needed for relative measurements like the difference of absolute values of the positive and the negative helicity states. Assuming conservatively $\Delta A_{\text{LR}}^e = 10^{-4}$ leads to

$$\delta \sin^2 \theta_{\text{eff}}^{\ell \text{ exp,ILC}} = 0.000013 , \quad (14)$$

more than a factor 10 better than the LEP/SLD result.

Within the SM, a full SM two-loop calculation for $\sin^2 \theta_{\text{eff}}^\ell$ is available, which is supplemented by the same type of three- and four-loop corrections as for M_W . This yields an intrinsic uncertainty of [22, 23]

$$\delta \sin^2 \theta_{\text{eff}}^{\ell \text{ SM,theo}} = 4.5 \times 10^{-5} , \quad (15)$$

which is mainly due to missing $\mathcal{O}(\alpha^2\alpha_s)$, $\mathcal{O}(N_f^3\alpha^3)$ and $\mathcal{O}(N_f^2\alpha^3)$ contributions. Assuming that these corrections will be calculated in the future, this error can be reduced to

$$\delta \sin^2 \theta_{\text{eff}}^{\ell\text{SM,theo,fut}} \approx 1.5 \times 10^{-5} . \quad (16)$$

Within the MSSM the intrinsic uncertainty increases relative to the SM due to the additional unknown higher-order corrections to [24]

$$\delta \sin^2 \theta_{\text{eff}}^{\ell\text{MSSM,theo}} = (5 - 7) \times 10^{-5} , \quad (17)$$

depending on the relevant SUSY mass scales. In the future one can expect a reduction to

$$\delta \sin^2 \theta_{\text{eff}}^{\ell\text{MSSM,theo,fut}} = (2.5 - 3.5) \times 10^{-5} . \quad (18)$$

The current parametric uncertainties (see the previous subsection) read

$$\delta \sin^2 \theta_{\text{eff}}^{\ell\text{para},m_t} = 7 \times 10^{-5}, \quad \delta \sin^2 \theta_{\text{eff}}^{\ell\text{para},\Delta\alpha_{\text{had}}} = 3.6 \times 10^{-5}, \quad \delta \sin^2 \theta_{\text{eff}}^{\ell\text{para},M_Z} = 1.4 \times 10^{-5} , \quad (19)$$

to be improved in the future (see the previous subsection) to

$$\delta \sin^2 \theta_{\text{eff}}^{\ell\text{para,fut},m_t} = 0.4 \times 10^{-5}, \quad \delta \sin^2 \theta_{\text{eff}}^{\ell\text{para,fut},\Delta\alpha_{\text{had}}} = 1.8 \times 10^{-5} . \quad (20)$$

The parametric uncertainties induced by M_Z and in particular $\Delta\alpha_{\text{had}}$, even assuming the future precision, are at or even slightly above the GigaZ precision of $\sin^2 \theta_{\text{eff}}^{\ell}$. Consequently, it will be very challenging to fully exploit the GigaZ precision.

In Fig. 2 we compare the SM and the MSSM predictions for M_W and $\sin^2 \theta_{\text{eff}}^{\ell}$ as obtained from scatter data similar to the one used in Fig. 1. The predictions within the two models give rise to two bands in the M_W – $\sin^2 \theta_{\text{eff}}^{\ell}$ plane with only a relatively small overlap region (indicated by a dark-shaded (blue) area). The parameter region shown in the SM (the medium-shaded (red) and dark-shaded (blue) bands) arises from varying the mass of the SM Higgs boson, from $M_H^{\text{SM}} = 114$ GeV, the old LEP exclusion bound [25] (lower edge of the dark-shaded (blue) area), to 400 GeV (upper edge of the medium-shaded (red) area), and from varying m_t in the range of $m_t = 165 \dots 175$ GeV. The value of $M_H^{\text{SM}} \sim 125.5$ GeV corresponds roughly to the dark-shaded (blue) strip. The light shaded (green) and the dark-shaded (blue) areas indicate allowed regions for the unconstrained MSSM, where no restriction on the light \mathcal{CP} -even Higgs mass has been applied. Including a Higgs mass measurement into the MSSM scan would cut away small part at the lower edge of the light shaded (green) area.

The 68% C.L. experimental results for M_W and $\sin^2 \theta_{\text{eff}}^{\ell}$ are indicated in the plot. The center ellipse corresponds to the current world average given in Eq. (9). Also shown are the error ellipses corresponding to the two individual most precise measurements of $\sin^2 \theta_{\text{eff}}^{\ell}$, based on A_{LR}^e by SLD and A_{FB}^b by LEP, corresponding to Eqs. (10), (11). The first (second) value prefers a value of $M_H^{\text{SM}} \sim 32(437)$ GeV [26]. The two measurements differ by more than 3σ . The averaged value of $\sin^2 \theta_{\text{eff}}^{\ell}$, as given in Eq. (9), prefers $M_H^{\text{SM}} \sim 110$ GeV [26]. The anticipated improvement with the ILC/GigaZ measurements, indicated as small ellipse, is

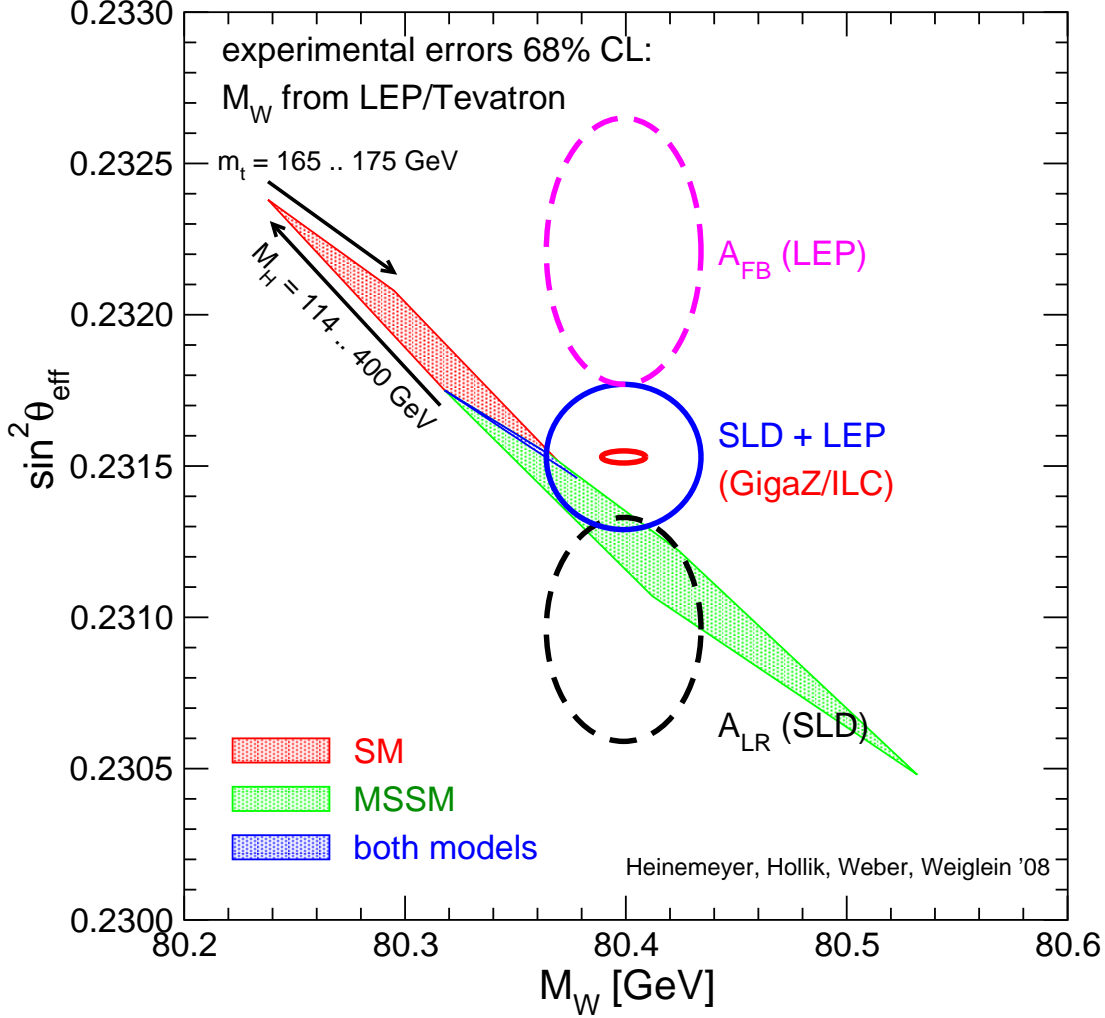


Figure 2: MSSM parameter scan for M_W and $\sin^2 \theta_{\text{eff}}^{\ell}$ over ranges similar to Fig. 1 with $m_t = 165 \dots 175$ GeV. Today's 68% C.L. ellipses (from $A_{\text{FB}}^b(\text{LEP})$, $A_{\text{LR}}^e(\text{SLD})$ and the world average) are shown as well as the anticipated GigaZ/ILC precisions, drawn around today's central value.

shown around the current experimental central data. One can see that the current averaged value is compatible with the SM with $M_H^{\text{SM}} \sim 125.5$ GeV and with the MSSM. The value of $\sin^2 \theta_{\text{eff}}^{\ell}$ obtained from $A_{\text{LR}}^e(\text{SLD})$ clearly favors the MSSM over the SM. On the other hand, the value of $\sin^2 \theta_{\text{eff}}^{\ell}$ obtained from $A_{\text{FB}}^b(\text{LEP})$ together with the M_W data from LEP and the Tevatron would correspond to an experimentally preferred region that deviates from the predictions of both models. This unsatisfactory solution can only be resolved by new measurements, where the Z factory, i.e. the GigaZ option would be an ideal solution. Thus, the unclear experimental situation regarding the two single most precise measurements entering the combined value for $\sin^2 \theta_{\text{eff}}^{\ell}$ has a significant impact on the constraints that can be obtained from this precision observable on possible New Physics scenarios. Measurements at a new $e^+e^- Z$ factory, which could be realized in particular with the GigaZ option of the ILC, would be needed to resolve this issue. As indicated by the solid light shaded (red)

ellipse, the anticipated ILC/GigaZ precision of the combined $M_W\text{-}\sin^2\theta_{\text{eff}}^\ell$ measurement could put severe constraints on each of the models and resolve the discrepancy between the A_{FB}^b (LEP) and A_{LR}^e (SLD) measurements.

Besides the leptonic effective weak mixing angle, similar effective weak mixing angles, $\sin^2\theta_{\text{eff}}^f$, can be defined for the interaction of the Z boson with other fermion flavors f , $f \neq \ell$. The SM predictions for these quantities have been computed including two-loop corrections with at least one close fermion loop (i.e. the ‘‘bosonic’’ electroweak two-loop contributions without closed fermion loops are not available yet), as well as leading three-loop corrections [23,27]. The remaining intrinsic theoretical uncertainty is

$$\delta \sin^2\theta_{\text{eff}}^{f \neq \ell, \text{SM, theo}} \approx 5 \times 10^{-5} , \quad (21)$$

which will be sufficient for the foreseeable future since the experimental precision for $\sin^2\theta_{\text{eff}}^b$, $\sin^2\theta_{\text{eff}}^c$, etc. is more than an order of magnitude less than for the leptonic weak mixing angle [20].

Besides asymmetry observables, additional constraints can be obtained from (partial) Z boson decay widths. The two most relevant quantities in this context are the total decay width Γ_Z , which is determined from the lineshape of the cross section $\sigma_{e^+e^- \rightarrow f\bar{f}}(s)$, and the ratio $R_b \equiv \Gamma_{Z \rightarrow b\bar{b}}/\Gamma_{Z \rightarrow \text{hadrons}}$. In particular, R_b is sensitive to new physics in the third generation of fermions, which is not directly probed by M_W and $\sin^2\theta_{\text{eff}}^\ell$ [28]. The current experimental result for R_b is [20]

$$R_b^{\text{exp}} = 0.21629 \pm 0.00066 . \quad (22)$$

This value differs from the SM prediction by about two standard deviations, which can be interpreted in terms of shifted couplings of the Z -boson to left- and right-handed bottom quarks, $g_{L,R}^b$ [28], see Fig. 3.

Due to higher statistics, the ILC running in the GigaZ mode will be able to reduce the experimental error substantially to [18]

$$\delta R_b^{\text{exp, ILC}} = 0.00015 , \quad (23)$$

which, together with improved asymmetry measurements, will help to clearly identify or rule out a possible new physics effect in the $Zb\bar{b}$ couplings, see Fig. 3.

The currently most precise SM prediction includes fermionic two-loop corrections (i.e. two-loop diagrams with at least one closed fermion loop) and leading three-loop terms [29], with an intrinsic uncertainty of

$$\delta R_b^{\text{SM, theo}} \approx 2 \times 10^{-4} . \quad (24)$$

The leading unknown contributions are $\mathcal{O}(\alpha\alpha_s^2)$ and $\mathcal{O}(\alpha^2\alpha_s)$ terms. In contrast to $\sin^2\theta_{\text{eff}}^\ell$, the vertex corrections of this order for quark final states involve more complex diagram topologies, so that only an approximate calculation in terms of a large- m_t expansion may be feasible in the near future. This would reduce the theory uncertainty to

$$\delta R_b^{\text{SM, theo, fut}} = (0.5 - 1) \times 10^{-4} . \quad (25)$$

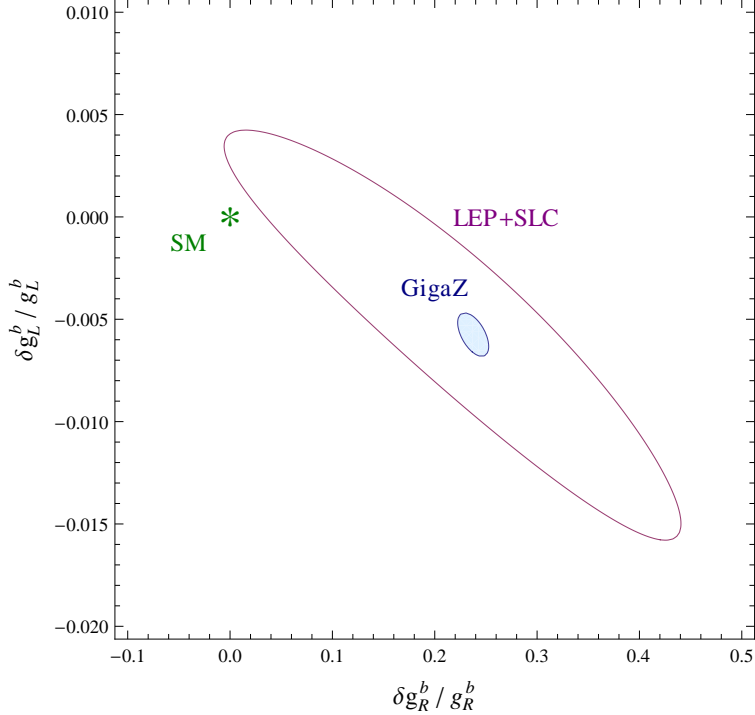


Figure 3: 95% C.L. level regions for the left- and right-handed $Zb\bar{b}$ couplings based on current experimental results from LEP/SLC and projected precision for GigaZ/ILC (assuming the same central values). The regions reflect experimental errors only. $\delta g_{L,R}^b = 0$ corresponds to the SM prediction (green star).

The current parametric uncertainties of R_b are small:

$$\delta R_b^{\text{para}, m_t} = 3.5 \times 10^{-5}, \quad \delta R_b^{\text{para}, \Delta\alpha_{\text{had}}} = 1.2 \times 10^{-6}, \quad \delta R_b^{\text{para}, M_Z} = 1.4 \times 10^{-6}, \quad (26)$$

and thus they do not pose any limit to future improvements.

The total Z width, Γ_Z , has been measured with high precision at LEP [20],

$$\Gamma_Z^{\text{exp}} = 2.4952 \pm 0.0023 \text{ GeV}, \quad (27)$$

which is mainly limited by the calibration and temporal fluctuations of the center-of-mass energy [20]. Therefore, the experimental precision is expected to improve only moderately at the GigaZ run of the ILC. A reasonable estimate [18] gives

$$\delta\Gamma_Z^{\text{exp, ILC}} = 0.001 \text{ GeV}. \quad (28)$$

For the calculation of Γ_Z in the SM, only an approximate result for the electroweak two-loop corrections in the limit of large m_t is known [30]. The remaining $\mathcal{O}(N_f\alpha^2)$ may be relatively large, as turned out to be the case for R_b [29]. Assuming the same relative size of the these corrections as for R_b , this leads to a current intrinsic uncertainty of a few MeV, which is by far dominant compared to missing three-loop contributions. However, the $\mathcal{O}(N_f\alpha^2)$ correction can be computed with existing methods without conceptual difficulties. The remaining intrinsic uncertainty is estimated to be

$$\delta\Gamma_Z^{\text{SM, theo, fut}} < 1 \text{ MeV}. \quad (29)$$

4.3 The top quark mass

The mass of the top quark, m_t , is a fundamental parameter of the electroweak theory. It is by far the heaviest of all quark masses and it is also larger than the masses of all other known fundamental particles. The large value of m_t gives rise to a large coupling between the top quark and the Higgs boson and is furthermore important for flavor physics. It could therefore provide a window to new physics. The top-quark mass also plays an important role in electroweak precision physics, as a consequence in particular of non-decoupling effects being proportional to powers of m_t . A precise knowledge of m_t is therefore indispensable in order to have sensitivity to possible effects of new physics in electroweak precision tests, see Eqs. (7), (8), (19), (20).

The current world average for the top-quark mass from the measurement at the Tevatron is [31],

$$m_t^{\text{exp}} = 173.2 \pm 0.9 \text{ GeV} . \quad (30)$$

The prospective accuracy at the LHC is $\delta m_t^{\text{exp}} \approx 1 \text{ GeV}$, while at the ILC a very precise determination of m_t with an accuracy of

$$\delta m_t^{\text{exp,ILC}} = 0.1 \text{ GeV} \quad (31)$$

will be possible. This uncertainty contains both the experimental error of the mass parameter extracted from the $t\bar{t}$ threshold measurements at the ILC and the envisaged theoretical uncertainty from its transition into a suitable short-distance mass (like the $\overline{\text{MS}}$ mass).

The relevance of the m_t precision as parametric uncertainty has been discussed for the W boson mass, M_W , in Sect. 4.1, and for the effective leptonic weak mixing angle, $\sin^2 \theta_{\text{eff}}^{\ell}$, in Sect. 4.2.

Because of its large mass, the top quark is expected to have a large Yukawa coupling to Higgs bosons, being proportional to m_t . In each model where the Higgs boson mass is not a free parameter but predicted in terms of the other model parameters (as e.g. in the MSSM), the diagram in Fig. 4 contributes to the Higgs mass. This diagram gives rise to a leading m_t contribution of the form

$$\Delta M_H^2 \sim G_F N_C C m_t^4 , \quad (32)$$

where G_F is the Fermi constant, N_C is the color factor, and the coefficient C depends on the specific model. Thus the experimental error of m_t necessarily leads to a parametric error in the Higgs boson mass evaluation.

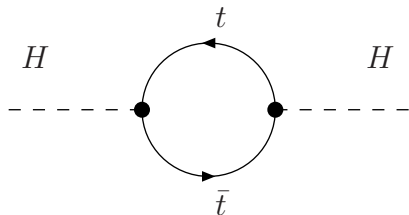


Figure 4: Loop contribution of the top quark to the Higgs boson mass.

Taking the MSSM as a specific example (including also the scalar top contributions and the appropriate renormalization) $N_C C$ is given for the light \mathcal{CP} -even Higgs boson mass in

leading logarithmic approximation by

$$N_C C = \frac{3}{\sqrt{2} \pi^2 \sin^2 \beta} \log \left(\frac{m_{\tilde{t}_1} m_{\tilde{t}_2}}{m_t^2} \right). \quad (33)$$

Here $m_{\tilde{t}_{1,2}}$ denote the two masses of the scalar tops. The current precision of $\delta m_t \sim 1$ GeV leads to an uncertainty of $\sim 2.5\%$ in the prediction of M_H , while the ILC will yield a precision of $\sim 0.2\%$. These uncertainties have to be compared with the anticipated precision of the future Higgs boson mass measurements. With a precision of $\delta M_H^{\text{exp,LHC}} \approx 0.2$ GeV the relative precision is at the level of $\sim 0.2\%$. It is apparent that only the ILC precision of m_t will yield a parametric error small enough to allow a precise comparison of the Higgs boson mass prediction and its experimental value (keeping also in mind the intrinsic theoretical uncertainties on M_H , see, e.g., Ref. [32] for the case of the MSSM).

4.4 The strong coupling constant

The GigaZ run can offer complementary information on α_s . It was shown [33] that a measurement of $R_l := \Gamma(Z \rightarrow \text{hadrons})/\Gamma(Z \rightarrow \text{leptons})$ down to $\delta R_l/R_l = \pm 0.05\%$ at GigaZ would provide a clean determination of α_s with an uncertainty of

$$\delta \alpha_s^{\text{exp,ILC}} \approx 0.001. \quad (34)$$

Since α_s enters (at least at the two-loop level) the radiative corrections to precision observables, it is important to control α_s effects to avoid confusion with other parametric uncertainties.

4.5 The Higgs boson mass

The observation of a new particle compatible with a Higgs boson of mass ~ 125 GeV is a major breakthrough in particle physics. It is of the greatest priority to measure the properties of this new particle with highest precision. Only high accuracy measurements may reveal the true nature of electroweak symmetry breaking and the fundamental structure of matter. The following questions can be addressed at the ILC:

- What are the couplings of the newly discovered particle to the known SM particles? Are the couplings to each particle proportional to the particle's mass?
- What is the mass and width of the newly discovered particle? What are the spin and CP quantum numbers?
- What is the self-coupling of the newly discovered particle? Is the measurement consistent with the predictions from a Higgs potential?
- Is the newly discovered particle a fundamental scalar as in the SM, or is only one out of several (similar) particles, potentially from scalar doublet, triplets, ...? Is the newly discovered particle composite?
- Does the newly discovered particle mix with new scalars of exotic origin, for instance with a radion of extra-dimensional models?

Any of these measurements may yield deviations from the SM predictions.

The Higgs boson mass plays a crucial role. Within the SM it was the last unknown parameter and can be tested against indirect determinations, see the next subsection. Within BSM models in which the mass can be calculated, the measured value can be compared to this prediction, where a precise knowledge of the top-quark mass is crucial, see Sect. 4.3.

4.6 Global electroweak fits

The precise determination of the top quark mass, together with improved measurements of the W boson mass, M_W , and the effective weak leptonic mixing angle, $\sin^2 \theta_{\text{eff}}^\ell$, can probe the quantum corrections of the SM and any other BSM model. The most important current and future uncertainties are summarized in Tabs. 2, (3).

| obs \ prec | today | ILC/GigaZ | SM theo | SM fut | MSSM theo | MSSM fut |
|---|-------|-----------|---------|--------|-----------|-----------|
| M_W [MeV] | 15 | 5 – 6 | 4 | 1 | 5 – 10 | 3 – 5 |
| $\sin^2 \theta_{\text{eff}}^\ell$ [10^{-5}] | 16 | 1.3 | 4.7 | 1.5 | 5 – 7 | 2.5 – 3.5 |
| m_t [GeV] | 0.9 | 0.1 | | | | |

Table 2: Precision of M_W , $\sin^2 \theta_{\text{eff}}^\ell$ and m_t : today's experimental precision, future precision from ILC/GigaZ measurements, intrinsic uncertainties from unknown higher-order corrections in the SM today and in the future, in the MSSM today and in the future.

| obs \ prec | δm_t | $\delta \Delta \alpha_{\text{had}}$ | δM_Z | $\delta m_{t,\text{fut}}$ | $\delta \Delta \alpha_{\text{had},\text{fut}}$ |
|---|--------------|-------------------------------------|--------------|---------------------------|--|
| M_W [MeV] | 5.5 | 2 | 2.5 | 1 | 1 |
| $\sin^2 \theta_{\text{eff}}^\ell$ [10^{-5}] | 7 | 3.6 | 1.4 | 0.4 | 1.8 |

Table 3: Parametric uncertainties of M_W and $\sin^2 \theta_{\text{eff}}^\ell$: today's experimental results using $\delta m_t^{\text{exp}} = 0.9$ GeV, $\delta(\Delta \alpha_{\text{had}}) = 10^{-4}$ and $\delta M_Z = 2.1$ MeV; future expectations use $\delta m_t^{\text{exp,ILC}} = 0.1$ GeV, $\delta(\Delta \alpha_{\text{had}})^{\text{fut}} = 5 \times 10^{-5}$.

Within the SM it is possible to predict the mass of the Higgs boson from its contribution to the prediction of EWPO, see Ref. [34] and references therein. With the current uncertainties¹ this leads to [34]

$$M_H^{\text{SM ind}} = 94_{-24}^{+29} \text{ GeV} , \quad (35)$$

as it is shown in the left plot of Fig. 5. The left yellow (shaded) area is excluded by LEP SM Higgs searches [25]. The right yellow (shaded) area is excluded by LHC SM Higgs searches.

Going to the ILC/GigaZ accuracy the indirect determination can reach a precision of

$$\delta M_H^{\text{SM ind,ILC}} \approx \pm 10 \text{ GeV} , \quad (36)$$

¹ $\delta M_W^{\text{SM,theo,fut}} = 2$ MeV has been assumed, having a minor impact on the results.

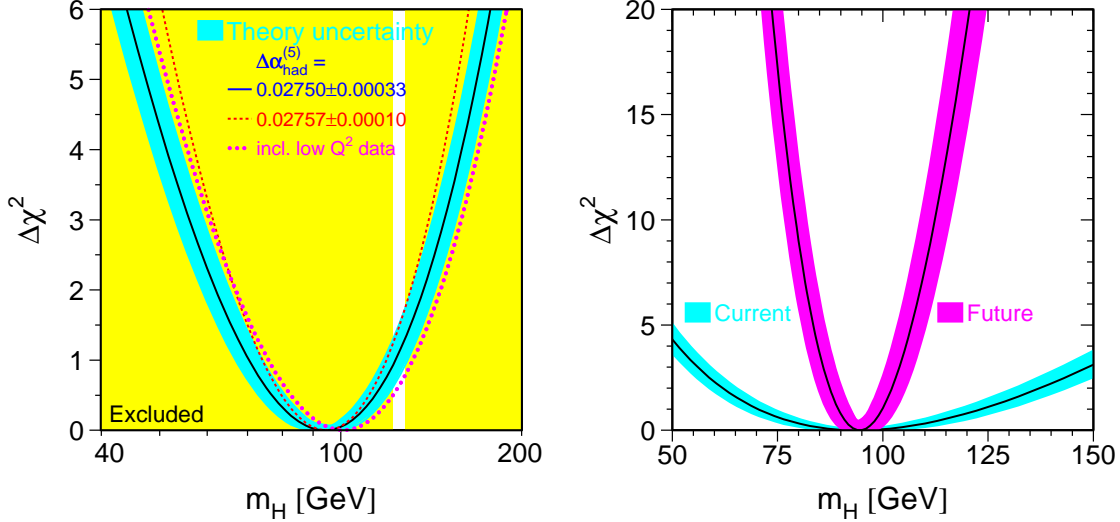


Figure 5: Indirect determination of M_H in the SM with current precision [34] (left) and future ILC/GigaZ precision [35] (right plot).

as it is shown in the right plot of Fig. 5 [35]. Any deviation of the indirectly determined mass from the directly measured value will indicate the presence of new physics scales beyond the SM. Similarly, the quantum effects in the MSSM can be tested to a very high precision [14].

5 Gauge boson couplings

Another possibility to search for new physics in the electroweak sector is the precision investigation of the couplings of the SM gauge bosons. At the ILC at tree-level, the incoming leptons interact via an exchange of an electroweak gauge boson. This allows for precise studies of trilinear gauge couplings in $e^+e^- \rightarrow W^+W^-$ as well as quartic gauge couplings occurring in a variety of final states like $e^+e^- \rightarrow VV$ where VV can be $\gamma\gamma$ or ZZ , or $e^+e^- \rightarrow VVV$ with VVV being WWZ or $WW\gamma$.

One advantage of the ILC over hadron collider measurements is the absence of parton distribution functions such that the center-of-mass energy of the scattering process is exactly known. Together with the tunable beam energy this allows to measure precisely the resonances. A second advantage is the clean environment of the ILC and the untriggered data taking.

The trilinear electroweak gauge couplings can parametrize the Lagrangian [36]

$$\begin{aligned} \mathcal{L}_{\text{TGC}} = & ig_{WWV} \left(g_1^V (W_{\mu\nu}^+ W^{-\mu} - W^{+\mu} W_{\mu\nu}^-) V^\nu + \kappa^V W_\mu^+ W_\nu^- V^{\mu\nu} + \frac{\lambda^V}{M_W^2} W_\mu^{\nu+} W_\nu^{-\rho} V_\rho^\mu \right. \\ & \left. + ig_4^V W_\mu^+ W_\nu^- (\partial^\mu V^\nu + \partial^\nu V^\mu) - ig_5^V \epsilon^{\mu\nu\rho\sigma} (W_\mu^+ \partial_\rho W_\nu^- - \partial_\rho W_\mu^+ W_\nu^-) V_\sigma \right) \end{aligned}$$

$$+\tilde{\kappa}^V W_\mu^+ W_\nu^- \tilde{V}^{\mu\nu} + \frac{\tilde{\lambda}^V}{M_W^2} W_\mu^{\nu+} W_\nu^{-\rho} \tilde{V}_\rho^\mu \Big), \quad (37)$$

with $V = \gamma, Z$; $W_{\mu\nu}^\pm = \partial_\mu W_\nu^\pm - \partial_\nu W_\mu^\pm$, $V_{\mu\nu} = \partial_\mu V_\nu - \partial_\nu V_\mu$ and $\tilde{V}_{\mu,\nu} = \epsilon_{\mu\nu\rho\sigma} V_{\rho\sigma}/2$. (Similarly a Lagrangian for quartic gauge couplings can be defined [37].) For the SM the couplings in Eq. (37) are given by

$$g_1^{\gamma,Z} = \kappa^{\gamma,Z} = 1, \quad g_{4,5}^{\gamma,Z} = \tilde{\kappa}^{\gamma,Z} = 1, \quad \lambda^{\gamma,Z} = \tilde{\lambda}^{\gamma,Z} = 0. \quad (38)$$

The couplings among the electroweak gauge bosons are directly given by the structure of the gauge group, see the previous section. This structure can thus directly be determined by a measurement of the gauge boson interactions. Particularly sensitive is the process $e^+e^- \rightarrow W^+W^-$, since any ‘‘naive’’ change in the gauge couplings would lead to a violation of unitarity, and small changes lead to relatively large variations. Electroweak precision observables together with the LEP data yield the strongest constraints on anomalous couplings [38,39]. For the triple gauge couplings the bounds are [39]

$$\begin{aligned} \Delta g_1^Z &= -0.033 \pm 0.031, \\ \Delta \kappa_\gamma &= 0.056 \pm 0.056, \\ \Delta \kappa_Z &= -0.0019 \pm 0.044, \\ \lambda_\gamma &= -0.036 \pm 0.034, \\ \lambda_Z &= 0.049 \pm 0.045. \end{aligned} \quad (39)$$

Turning to the ILC, the different types of couplings can be disentangled experimentally by analyzing the production angle distribution of the W boson and the structure of the W polarization, which can be obtained from the distributions of the decay angles. Anomalous couplings for $WW\gamma$ and WWZ result in similar final state distributions. However, using beam polarization, they can be disentangled, where a large beam polarization, in particular for the left-handed e^- is required. Also positron polarization is required for an optimal resolution [5]. A fast detector simulation analysis was performed for $\sqrt{s} = 500$ GeV and 800 GeV [40]. The results for single parameter fits are shown in Tab. 4. Correlations in the multi-parameter fits were taken into account where possible. For $\sqrt{s} = 800$ GeV they are relatively small, not increasing the uncertainties by more than $\sim 20\%$. At $\sqrt{s} = 500$ GeV the effect is larger, and uncertainties can increase by up to a factor of two, see also Ref. [41].

Figure 6 compares the expected precision for the κ_γ and λ_γ measurements at various colliders [42]. The advantage of ILC is clearly seen for the κ couplings. It is an example of new physics effects with lower mass dimension operators, for which precise measurements at low energies can be more effective than less precise measurements at higher energies.

6 Extra gauge bosons

The two-fermion processes $e^+e^- \rightarrow f\bar{f}$, where f is a quark or charged lepton, are especially powerful probes of TeV scale Z' s, extra dimensions, and other new physics leading to contact interactions such as quark or lepton compositeness.

| coupling | error $\times 10^{-4}$ | |
|------------------------|------------------------|----------------------|
| | $\sqrt{s} = 500$ GeV | $\sqrt{s} = 800$ GeV |
| Δg_1^Z | 15.5 | 12.6 |
| $\Delta \kappa_\gamma$ | 3.3 | 1.9 |
| λ_γ | 5.9 | 3.3 |
| $\Delta \kappa_Z$ | 3.2 | 1.9 |
| λ_Z | 6.7 | 3.0 |
| g_5^Z | 16.5 | 14.4 |
| g_4^Z | 45.9 | 18.3 |
| $\tilde{\kappa}_Z$ | 39.0 | 14.3 |
| $\tilde{\lambda}_Z$ | 7.5 | 3.0 |

Table 4: Results of the single parameter fits (1σ) to the different triple gauge couplings at the ILC for $\sqrt{s} = 500$ GeV with $\mathcal{L} = 500\text{fb}^{-1}$ and $\sqrt{s} = 800$ GeV with $\mathcal{L} = 1000\text{fb}^{-1}$; $\mathcal{P}_{e^-} = 80\%$ and $\mathcal{P}_{e^+} = 60\%$ has been used.

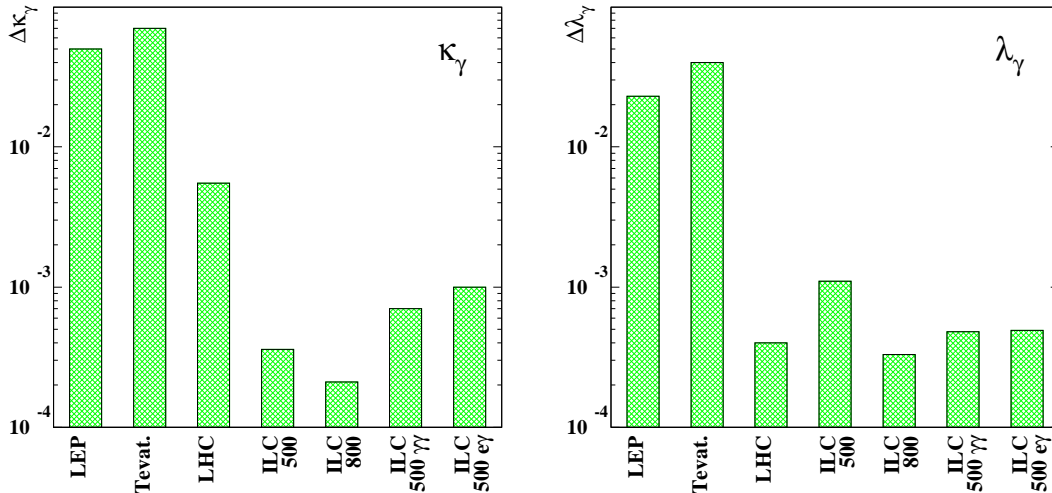


Figure 6: Comparison of $\Delta \kappa_\gamma$ and $\Delta \lambda_\gamma$ at different machines. For LHC and ILC three years of running are assumed (LHC: 300fb^{-1} , ILC $\sqrt{s} = 500$ GeV: 500fb^{-1} , ILC $\sqrt{s} = 800$ GeV: 1000fb^{-1}). If available the results from multi-parameter fits have been used. Taken from Ref. [42].

6.1 Z' Gauge Bosons

Additional $U(1)'$ gauge symmetries occur in many extensions of the standard model (SM), often with the Z' mass at the TeV scale². For example, grand unified theories and string constructions often involve large underlying gauge groups, which can easily leave behind (remnant) $U(1)'$ factors in addition to the SM group when broken. Some string constructions, such as the type IIA intersecting-brane theories, are based on $U(n) = SU(n) \times U(1)$ factors. Although the $U(1)$ factors are typically anomalous, linear combinations (in addition to weak

²For reviews, see, e.g., [43–47]. For previous studies in e^+e^- colliders, see [2, 48–55].

hypercharge) may be non-anomalous and survive to low energies. In supersymmetric models with an additional $U(1)'$ both the $SU(2) \times U(1)$ and $U(1)'$ breaking scales are typically set by the supersymmetry-breaking soft parameters (unless there are flat directions), and the $U(1)'$ can provide an elegant solution to the μ problem similar to the NMSSM.

$U(1)'$ s also occur in extended electroweak models, such as left-right symmetry, and in many alternative models of electroweak symmetry breaking (EWSB), such as various dynamical symmetry breaking or Little Higgs models. In some cases these feature enhanced couplings to the third generation. Although many of the alternative EWSB models are disfavored by the discovery of the Higgs-like boson at ~ 125 GeV, there still remains the possibility that the minimal Higgs model is only an approximation to an underlying alternative mechanism. Models in which the photon and Z propagate in extra dimensions involve Kaluza-Klein excitations, which could resemble a Z' . For a flat dimension of radius R , for example, the Kaluza-Klein mass scale is $M \sim R^{-1} \sim 2 \text{ TeV} \times (10^{-17} \text{ cm}/R)$. Extra (family non-universal) Z' s have also been invoked in connection with possible experimental anomalies, such as the still-unexplained forward-backward asymmetry in $t\bar{t}$ production reported by CDF and D0.

Z' s have also been motivated by other considerations, such as light weakly-coupled Z' s which could communicate with an otherwise dark sector. However, we concentrate on TeV-scale Z' s with electroweak-strength couplings, for which the ILC has a significant reach. We emphasize that the observation of such a Z' would have major consequences: most models are accompanied by extended Higgs and neutralino sectors and new exotic fermions (for anomaly cancellation), and may have implications for neutrino mass, electroweak baryogenesis, tree-level FCNC, and the mediation of supersymmetry breaking. An on-shell Z' could serve as a sparticle/exotics factory.

The effects of Z' s have been extensively searched for in precision electroweak physics, which limits any $Z - Z'$ mixing to a few parts in a thousand and places lower limits on $M_{Z'}$ ranging from a few hundred GeV to ~ 1 TeV for typical benchmark models [56, 57]. The mass limits were superseded by direct searches at the Tevatron and then the LHC for resonant Z' production with decays into dileptons or into $t\bar{t}$ or $b\bar{b}$ pairs. The current ATLAS and CMS lower limits from dileptons are in the 2-2.5 TeV range for benchmark models, with a future discovery reach of $\sim 4 - 5$ TeV for $\sqrt{s} = 14$ TeV and $\int \mathcal{L} = 100 \text{ fb}^{-1}$. For lower masses (up to around 2.5 TeV) there would be significant possibilities for discriminating between Z' models at the LHC utilizing forward-backward asymmetries, rapidity distributions, lineshape variables, other decay modes, τ polarization, associated production, and rare decays. However, for the larger masses favored by the present LHC constraints the diagnostic possibilities are more limited³.

The ILC has a significant reach for observing the effects of a Z' and discriminating between models due to the interference of a heavy virtual⁴ Z' with s -channel γ and Z exchange in the processes $e^+e^- \rightarrow f\bar{f}$, with $f = e, \mu, \tau, c$, and b (t -channel exchange must also be considered for $f = e$). For unpolarized beams the basic observables are the total cross sections, forward backward asymmetries, and τ polarization. Additional probes, including the polarization asymmetry and the forward-backward polarization asymmetry, become available for

³The LHC possibilities are extensively discussed in [46–49, 51, 58–70].

⁴Existing limits already exclude Z' s with electroweak couplings to charged leptons with mass light enough for resonant production at the ILC.

polarized e^\pm . The ability to polarize both beams leads to a larger effective polarization as well as providing an additional handle for new-physics identification and systematics effects.

Especially detailed studies of the ILC discovery potential and model discrimination have been carried out in [52] and [53]. The 95% C.L. discovery reach for the ILC for various benchmark models is shown in Figure 7, taken from [53]. It is seen that the reach for $\sqrt{s} = 0.5$ TeV and $\int \mathcal{L} = 500 \text{ fb}^{-1}$ is in the range 4-10 TeV for the models considered, increasing with beam polarization. For 1 TeV and 1000 fb^{-1} the range increases to around 6-15 TeV, well above the reach of the LHC.

The ILC also would allow excellent discrimination between Z' models. Of course, the cleanest identification would be for a relatively low mass Z' that had already been observed (and its mass determined) at the LHC. However, the diagnostic reach of the ILC extends much higher, almost up to the discovery reach, and far beyond the possibilities for the LHC. This is illustrated in Figure 8, taken from [53].

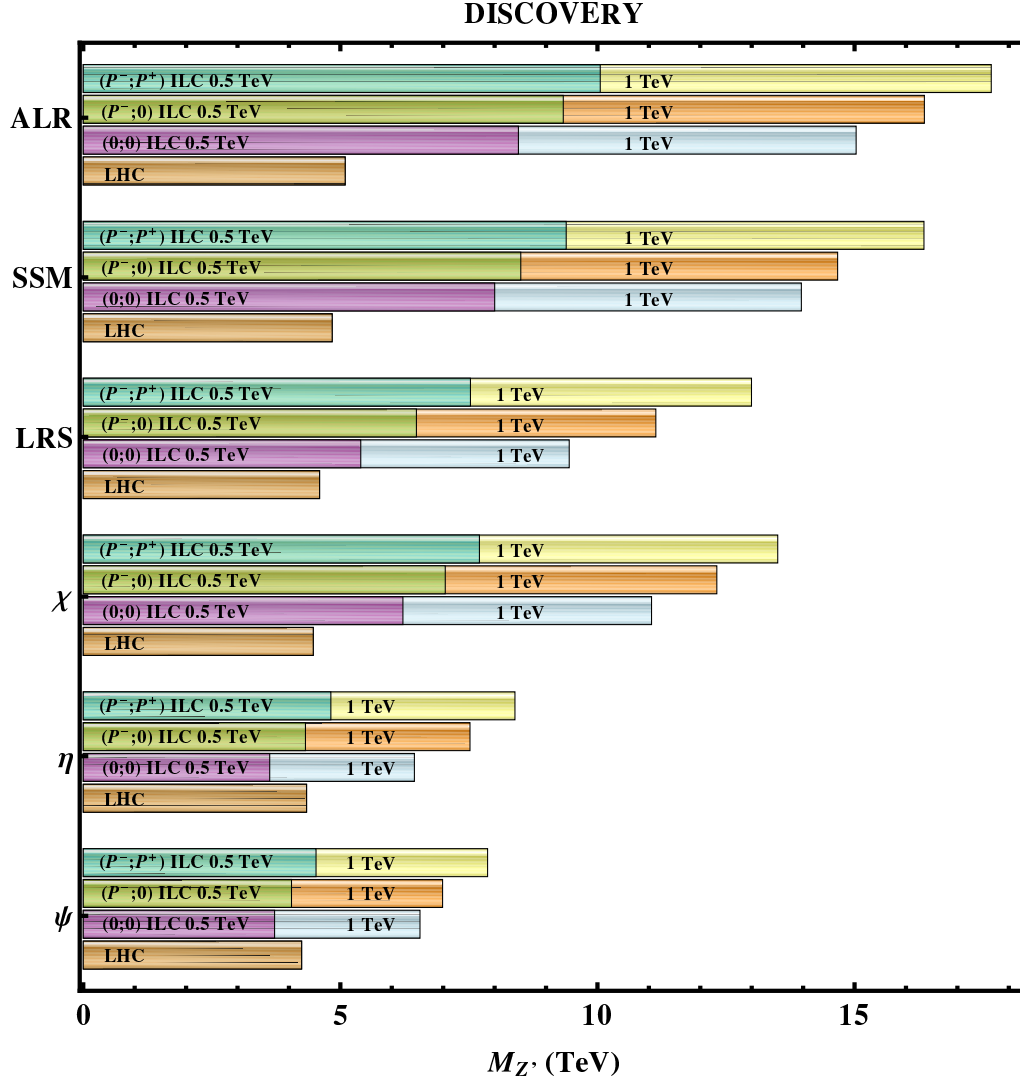


Figure 7: 95% C.L. discovery reach of the ILC for various benchmark Z' models at $\sqrt{s} = 0.5$ TeV (1 TeV), integrated luminosity 500 fb^{-1} (1000 fb^{-1}), and various polarization scenarios, from [53]. The nonzero polarizations are $|P^-| = 0.8$ and $|P^+| = 0.6$. Also shown is the LHC 5σ reach at $\sqrt{s} = 14$ TeV and $\int \mathcal{L} = 100 \text{ fb}^{-1}$.

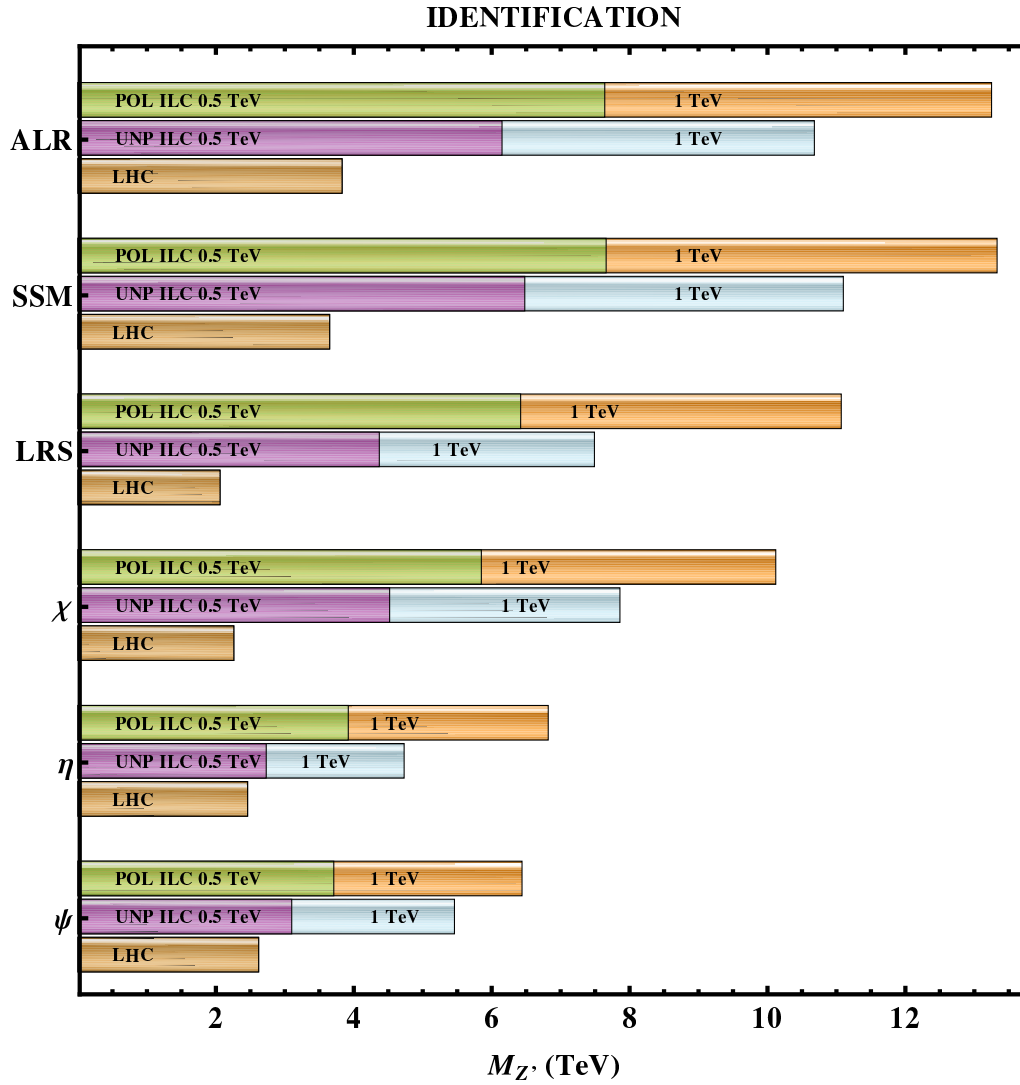


Figure 8: Reach for discriminating between the models shown at 95% C.L., from [53]. The energies and integrated luminosities are as in Figure 7, while UNP and POL refer respectively to no polarization, and to $|P^-| = 0.8$, $|P^+| = 0.6$.

6.2 W' Gauge Bosons

Heavy singly charged gauge bosons W' occur, for example, in $SU(2)_L \times SU(2)_R \times U(1)$ models (including left-right symmetric models), in many extended models of electroweak symmetry breaking (e.g., involving $SU(2)_1 \times SU(2)_2$ breaking to a diagonal subgroup), and as Kaluza-Klein excitations in models in which the W propagates in extra dimensions⁵.

W' couplings to the SM and other fermions are characterized by chirality (i.e., whether the couplings are to $V + A$, as in $SU(2)_L \times SU(2)_R \times U(1)$, or to $V - A$, as in the diagonal embeddings of $SU(2)$ or for Kaluza-Klein excitations); the analog of the CKM matrix for the quark currents; possible $W - W'$ mixing; and the W' gauge couplings. For $V + A$ couplings one must also specify whether the right-handed neutrinos ν_R are light (as for Dirac neutrinos or possibly for eV-scale “sterile” neutrinos) or heavy (as in an ordinary seesaw model). In the latter case, the ν_R could be TeV scale or lighter, or could be too heavy to produce at the LHC or other facilities.

The existing constraints are difficult to summarize because of the many possibilities mentioned above. There are significant limits on mass and mixing from β and μ decay and weak universality (from W' exchange and $W - W'$ mixing), from neutral meson mixing (from box diagrams), from the W mass and other precision electroweak, and from correlated $W' - Z'$ constraints in specific models. Depending on the couplings, these set lower limits on $M_{W'}$ ranging from several hundred GeV to around 2.5 TeV [67, 71–75].

At the Tevatron and LHC [71–73, 76–78] one can search for $W' \rightarrow \ell\nu$ for $V - A$ (or $V + A$ with light ν_R), or for $W' \rightarrow \ell\nu_R, \nu_R \rightarrow \ell jj$ for a heavy ν_R that is lighter than the W' . In all cases one can also utilize the nonleptonic decays such as $W' \rightarrow t\bar{b}$. The current CMS and ATLAS lower limits on $M_{W'}$ are around 3.35 TeV for $\ell\nu$ [79, 80], 2.5 TeV for kinematically allowed leptonic decays with a heavy neutrino [81, 82], and 1.8 TeV for non-leptonic decays [83, 84]. Most of these limits are based on only a fraction of the existing data. Higher energy and luminosity will presumably allow considerably improved sensitivity into the multi-TeV range. Additional information on the chirality, etc., may be obtained by leptonic decays, top polarization [71], associated $W't$ production [72], etc.

The ILC offers only limited possibilities for discovery or diagnostics of a W' . In particular, the process $e^-e^+ \rightarrow \nu\bar{\nu}\gamma$ could proceed via t -channel W' exchange (with the photon radiated from a charged particle). The sensitivity extends to around 6 TeV for $V - A$ and 1.9 TeV for $V + A$ with a light Dirac neutrino, assuming $\sqrt{s} = 1$ TeV, $\int \mathcal{L} = 500 \text{ fb}^{-1}$, high beam polarizations, and favorable assumptions concerning the coupling strength [85]. Although not competitive with the LHC for discovery, measurements of the cross section and left-right asymmetry in $\nu\bar{\nu}\gamma$ could help constrain the chirality.

7 Conclusions

We have reviewed the experimental conditions and prospects for the measurement of precision observables at the ILC.

The observables comprise the W boson mass, Z pole observables and in particular the effective weak leptonic mixing angle, $\sin^2 \theta_{\text{eff}}^\ell$, the top-quark mass (and other top related ob-

⁵For recent general discussions, see, e.g., [71–73], which contain references to earlier papers.

servables), the strong coupling constant, α_s , and the Higgs boson mass. These measurement of these observables will allow a test of the SM (or any other model) at the quantum level. In particular, the Higgs boson mass can be determined *indirectly*, which can be compared to the *directly* measured value.

In the case that the LHC will discover no additional new physics, i.e. only the full particle content of the SM would be discovered, the precision measurements at the ILC of the Higgs boson properties (in particular the couplings to other SM particles and to itself), together with the precision determinations of m_t , M_W , $\sin^2 \theta_{\text{eff}}^\ell$ etc. would constitute a clear way to search for new scales beyond the SM. Only the high anticipated precision would offer the opportunity to find traces of high scales beyond the direct kinematical reach of the LHC or the ILC.

We have also reviewed the prospects for the measurements of triple and quartic (SM) gauge boson couplings as well as the potential measurement of additional heavy gauge bosons. While currently no deviations in the couplings from the SM values can be observed, these measurements have the potential to find traces of physics beyond the SM. Scales even beyond 10 TeV can be probed in models with additional gauge bosons, far beyond the direct kinematical reach of the LHC or the ILC.

Acknowledgements

We acknowledge useful discussions with M. Grünewald, A H \ddot{o} cker and R. Kogler. The work of S.H. was supported in part by CICYT (grant FPA 2010–22163-C02-01) and by the Spanish MICINN’s Consolider-Ingenio 2010 Program under grant MultiDark CSD2009-00064.

References

- [1] Technical Design Report, The ILC Baseline Design, <https://forge.linearcollider.org/dist/20121210-CA-TDR2.pdf> (2013).
- [2] H. Baer *et al.*, “The International Linear Collider Technical Design Report - Volume 2: Physics“, arXiv:1306.6352 [hep-ex].
- [3] ILC Detector Baseline Document, <http://ific.uv.es/~fuster/DBD-Chapters/> (2013).
- [4] Parameters for the Linear Collider, http://www.fnal.gov/directorate/icfa/recent_lc_activities_files/para-Nov20-final.pdf (2003, updated 2006).
- [5] G. Moortgat-Pick, T. Abe, G. Alexander, B. Ananthanarayan, A. A. Babich, V. Bharadwaj, D. Barber and A. Bartl *et al.*, Phys. Rept. **460** (2008) 131 [hep-ph/0507011].
- [6] M. Beckmann, B. List, J. List, NIM paper.
- [7] K. Moenig, LC-PHSM-2000-060; A. Sailer, Diploma Thesis.
- [8] Tevatron Electroweak Working Group [CDF and D0 Collaborations], arXiv:1204.0042 [hep-ex].
- [9] J. Alcaraz *et al.* [ALEPH and DELPHI and L3 and OPAL and LEP Electroweak Working Group Collaborations], hep-ex/0612034.
- [10] G.W. Wilson, LC-PHSM-2001-009, see: <http://www-flc.desy.de/lcnotes/> .
- [11] A. Denner, S. Dittmaier, M. Roth and L. H. Wieders, Phys. Lett. B **612** (2005) 223 [Erratum-ibid. B **704** (2011) 667] [hep-ph/0502063].
- [12] A. Denner, S. Dittmaier, M. Roth and L. H. Wieders, Nucl. Phys. B **724** (2005) 247 [Erratum-ibid. B **854** (2012) 504] [hep-ph/0505042].
- [13] U. Baur, R. Clare, J. Erler, S. Heinemeyer, D. Wackerroth, G. Weiglein and D. R. Wood, eConf C **010630** (2001) P122 [hep-ph/0111314].
- [14] S. Heinemeyer, W. Hollik and G. Weiglein, Phys. Rept. **425** (2006) 265 [hep-ph/0412214].
- [15] M. Awramik, M. Czakon, A. Freitas and G. Weiglein, Phys. Rev. D **69** (2004) 053006 [hep-ph/0311148].
- [16] S. Heinemeyer, W. Hollik, D. Stockinger, A. M. Weber and G. Weiglein, JHEP **0608** (2006) 052 [arXiv:hep-ph/0604147].
- [17] S. Heinemeyer, G. Weiglein and L. Zeune, DESY 13–015, *in preparation*.
- [18] R. Hawkings and K. Mönig, EPJdirect C **8** (1999) 1 [arXiv:hep-ex/9910022].

- [19] S. Heinemeyer, Th. Mannel and G. Weiglein, Proceedings, Linear Collider Workshop Sitges 1999, arXiv:hep-ph/9909538.
- [20] S. Schael *et al.* [ALEPH and DELPHI and L3 and OPAL and SLD and LEP Electroweak Working Group and SLD Electroweak Group and SLD Heavy Flavour Group Collaborations], Phys. Rept. **427** (2006) 257 [hep-ex/0509008].
- [21] A. Blondel, Phys. Lett. B **202** (1988) 145 [Erratum-ibid. **208** (1988) 531].
- [22] M. Awramik, M. Czakon and A. Freitas, Phys. Lett. B **642**, 563 (2006) [hep-ph/0605339];
W. Hollik, U. Meier and S. Uccirati, Nucl. Phys. B **765**, 154 (2007) [hep-ph/0610312].
- [23] M. Awramik, M. Czakon and A. Freitas, JHEP **0611**, 048 (2006) [hep-ph/0608099].
- [24] S. Heinemeyer, W. Hollik, A. M. Weber and G. Weiglein, JHEP **0804** (2008) 039 [arXiv:0710.2972 [hep-ph]].
- [25] R. Barate *et al.* [LEP Working Group for Higgs boson searches and ALEPH and DELPHI and L3 and OPAL Collaborations], Phys. Lett. B **565** (2003) 61 [hep-ex/0306033].
- [26] M. Grünewald, *private communication*.
- [27] M. Awramik, M. Czakon, A. Freitas and B. A. Kniehl, Nucl. Phys. B **813** (2009) 174 [arXiv:0811.1364 [hep-ph]].
- [28] B. Batell, S. Gori and L.-T. Wang, JHEP **1301** (2013) 139 [arXiv:1209.6382 [hep-ph]];
D. Choudhury, A. Kundu and P. Saha, arXiv:1305.7199 [hep-ph];
M. Ciuchini, E. Franco, S. Mishima and L. Silvestrini, arXiv:1306.4644 [hep-ph].
- [29] A. Freitas and Y.-C. Huang, JHEP **1208** (2012) 050 [Erratum-ibid. **1305** (2013) 074] [arXiv:1205.0299 [hep-ph]].
- [30] J. Fleischer, O. V. Tarasov and F. Jegerlehner, Phys. Rev. D **51** (1995) 3820;
G. Degrandi and P. Gambino, Nucl. Phys. B **567** (2000) 3 [hep-ph/9905472].
- [31] [Tevatron Electroweak Working Group and CDF and D0 Collaborations], arXiv:1107.5255 [hep-ex]; arXiv:1305.3929 [hep-ex].
- [32] G. Degrandi, S. Heinemeyer, W. Hollik, P. Slavich and G. Weiglein, Eur. Phys. J. C **28** (2003) 133 [hep-ph/0212020].
- [33] J. Erler, S. Heinemeyer, W. Hollik, G. Weiglein and P. M. Zerwas, Phys. Lett. B **486** (2000) 125 [hep-ph/0005024].
- [34] S. Schael *et al.* [ALEPH and DELPHI and L3 and OPAL and LEP Electroweak Working Group Collaborations], arXiv:1302.3415 [hep-ex].
- [35] M. Grünewald, *priv. communication*;
G. Moortgat-Pick *et al.*, “LC review”, to appear in Eur. Phys. J. C .

- [36] K. Hagiwara, R. D. Peccei, D. Zeppenfeld and K. Hikasa, Nucl. Phys. B **282** (1987) 253.
- [37] M. Beyer, W. Kilian, P. Krstonosic, K. Monig, J. Reuter, E. Schmidt and H. Schroder, Eur. Phys. J. C **48** (2006) 353 [hep-ph/0604048].
- [38] C. P. Burgess, S. Godfrey, H. Konig, D. London and I. Maksymyk, Phys. Rev. D **49** (1994) 6115 [arXiv:hep-ph/9312291].
- [39] H. Aihara, T. Barklow, U. Baur, J. Busenitz, S. Errede, T. A. Fuess, T. Han and D. London *et al.*, [arXiv:hep-ph/9503425].
- [40] W. Menges, LC-PHSM-2001-022, see: www-flc.desy.de/lcnotes/ .
- [41] J. A. Aguilar-Saavedra *et al.* [ECFA/DESY LC Physics Working Group Collaboration], hep-ph/0106315.
- [42] G. Aarons *et al.* [ILC Collaboration], arXiv:0709.1893 [hep-ph].
- [43] M. Cvetic and S. Godfrey, In *Barklow, T.L. (ed.) et al.: Electroweak symmetry breaking and new physics at the TeV scale* 383-415 [hep-ph/9504216].
- [44] J. L. Hewett and T. G. Rizzo, Phys. Rept. **183** (1989) 193.
- [45] A. Leike, Phys. Rept. **317** (1999) 143 [hep-ph/9805494].
- [46] P. Langacker, Rev. Mod. Phys. **81** (2009) 1199 [arXiv:0801.1345 [hep-ph]].
- [47] P. Nath, B. D. Nelson, H. Davoudiasl, B. Dutta, D. Feldman, Z. Liu, T. Han and P. Langacker *et al.*, Nucl. Phys. Proc. Suppl. **200-202** (2010) 185 [arXiv:1001.2693 [hep-ph]].
- [48] F. Del Aguila and M. Cvetic, Phys. Rev. D **50** (1994) 3158 [hep-ph/9312329].
- [49] F. Del Aguila, M. Cvetic and P. Langacker, Phys. Rev. D **52** (1995) 37 [hep-ph/9501390].
- [50] E. Accomando *et al.* [ECFA/DESY LC Physics Working Group Collaboration], Phys. Rept. **299** (1998) 1 [hep-ph/9705442].
- [51] G. Weiglein *et al.* [LHC/LC Study Group Collaboration], Phys. Rept. **426** (2006) 47 [hep-ph/0410364].
- [52] S. Godfrey, P. Kalyniak and A. Tomkins, hep-ph/0511335.
- [53] P. Osland, A. A. Pankov and A. V. Tsytrinov, Eur. Phys. J. C **67** (2010) 191 [arXiv:0912.2806 [hep-ph]].
- [54] L. Linssen, A. Miyamoto, M. Stanitzki and H. Weerts, arXiv:1202.5940 [physics.ins-det].
- [55] M. Battaglia, F. Coradeschi, S. De Curtis and D. Dominici, arXiv:1203.0416 [hep-ph].

- [56] J. Erler, P. Langacker, S. Munir and E. Rojas, JHEP **0908** (2009) 017 [arXiv:0906.2435 [hep-ph]].
- [57] R. Diener, S. Godfrey and I. Turan, Phys. Rev. D **86** (2012) 115017 [arXiv:1111.4566 [hep-ph]].
- [58] P. Langacker, R. W. Robinett and J. L. Rosner, Phys. Rev. D **30** (1984) 1470.
- [59] F. del Aguila, M. Cvetič and P. Langacker, Phys. Rev. D **48** (1993) 969 [hep-ph/9303299].
- [60] M. Dittmar, A. -S. Nicollerat and A. Djouadi, Phys. Lett. B **583** (2004) 111 [hep-ph/0307020].
- [61] J. Kang and P. Langacker, Phys. Rev. D **71** (2005) 035014 [hep-ph/0412190].
- [62] F. Petriello and S. Quackenbush, Phys. Rev. D **77** (2008) 115004 [arXiv:0801.4389 [hep-ph]].
- [63] S. Godfrey and T. A. W. Martin, Phys. Rev. Lett. **101** (2008) 151803 [arXiv:0807.1080 [hep-ph]].
- [64] P. Osland, A. A. Pankov, A. V. Tsytrinov and N. Paver, Phys. Rev. D **79** (2009) 115021 [arXiv:0904.4857 [hep-ph]].
- [65] Y. Li, F. Petriello and S. Quackenbush, Phys. Rev. D **80** (2009) 055018 [arXiv:0906.4132 [hep-ph]].
- [66] R. Diener, S. Godfrey and T. A. W. Martin, arXiv:0910.1334 [hep-ph].
- [67] F. del Aguila, J. de Blas and M. Perez-Victoria, JHEP **1009** (2010) 033 [arXiv:1005.3998 [hep-ph]].
- [68] C. -F. Chang, K. Cheung and T. -C. Yuan, JHEP **1109** (2011) 058 [arXiv:1107.1133 [hep-ph]].
- [69] J. Erler, P. Langacker, S. Munir and E. Rojas, JHEP **1111** (2011) 076 [arXiv:1103.2659 [hep-ph]].
- [70] C. -W. Chiang, N. D. Christensen, G. -J. Ding and T. Han, Phys. Rev. D **85** (2012) 015023 [arXiv:1107.5830 [hep-ph]].
- [71] S. Gopalakrishna, T. Han, I. Lewis, Z. -g. Si and Y. -F. Zhou, Phys. Rev. D **82** (2010) 115020 [arXiv:1008.3508 [hep-ph]].
- [72] M. Frank, A. Hayreter and I. Turan, Phys. Rev. D **83** (2011) 035001 [arXiv:1010.5809 [hep-ph]].
- [73] M. Schmaltz and C. Spethmann, JHEP **1107** (2011) 046 [arXiv:1011.5918 [hep-ph]].

- [74] K. Hsieh, K. Schmitz, J. -H. Yu and C. -P. Yuan, Phys. Rev. D **82** (2010) 035011 [arXiv:1003.3482 [hep-ph]].
- [75] M. Frank, A. Hayreter and I. Turan, Phys. Rev. D **82** (2010) 033012 [arXiv:1005.3074 [hep-ph]].
- [76] Q. -H. Cao, Z. Li, J. -H. Yu and C. P. Yuan, Phys. Rev. D **86** (2012) 095010 [arXiv:1205.3769 [hep-ph]].
- [77] C. Du, H. -J. He, Y. -P. Kuang, B. Zhang, N. D. Christensen, R. S. Chivukula and E. H. Simmons, Phys. Rev. D **86** (2012) 095011 [arXiv:1206.6022 [hep-ph]].
- [78] D. Duffty and Z. Sullivan, Phys. Rev. D **86** (2012) 075018 [arXiv:1208.4858 [hep-ph]].
- [79] The CMS Collaboration, CMS-PAS-EXO-12-060.
- [80] G. Aad *et al.* [ATLAS Collaboration], Eur. Phys. J. C **72** (2012) 2241 [arXiv:1209.4446 [hep-ex]].
- [81] G. Aad *et al.* [ATLAS Collaboration], Eur. Phys. J. C **72** (2012) 2056 [arXiv:1203.5420 [hep-ex]].
- [82] The CMS Collaboration, CMS-PAS-EXO-12-017.
- [83] S. Chatrchyan *et al.* [CMS Collaboration], Phys. Lett. B **718** (2013) 1229 [arXiv:1208.0956 [hep-ex]].
- [84] The ATLAS Collaboration, ATLAS-CONF-2013-050.
- [85] S. Godfrey, P. Kalyniak, B. Kamal and A. Leike, Phys. Rev. D **61** (2000) 113009 [hep-ph/0001074].